water

MDPI

Article

Elucidating the Degradation of Naphthalene in Fenton-like Processes Coupled with Various Sulfur-Iron Materials: Performance and Mechanisms

Guilu Zeng [1,2], Chi Zhang [1], Shuguang Lyu [2] and Xia Ma [1,*]

[1] Zhejiang Key Laboratory of Ecological Environmental Damage Control and Value Transformation, Ecological and Environmental Science and Research Institute of Zhejiang Province, Hangzhou 310007, China; 17717427293@163.com (G.Z.); zchi@outlook.com (C.Z.)

[2] State Environmental Protection Key Laboratory of Environmental Risk Assessment and Control on Chemical Process, East China University of Science and Technology, Shanghai 200237, China; lvshuguang@ecust.edu.cn

* Correspondence: maxia0519@163.com; Tel./Fax: +86-571-87997808

Abstract

In this work, three sulfur-iron materials (sulfide-modified nanoscale zerovalent iron (S-nZVI), ferrous sulfide (FeS), and pyrite (FeS_2)) were employed to enhance the Fenton process for naphthalene (NAP) degradation. The enhancement performance and mechanisms of S-nZVI, FeS, and FeS_2 were investigated and compared. The results showed that NAP removal was enhanced from 56.4% in the H_2O_2/Fe(II) system to 88.6%, 83.0%, and 89.1% with the addition of S-nZVI, FeS, and FeS_2, respectively. Three sulfur-iron materials could all reduce Fe(III) produced in aqueous solution, regenerate Fe(II), and slow down the precipitation of dissolved iron. In addition, the addition of sulfur-iron materials could promote the generation of hydroxyl radical (HO•), thus intensifying the degradation of NAP. The results of scavenging tests indicated that HO• was the dominant reactive oxygen species (ROS) for NAP removal, while superoxide radical (O_2^-•) also participated. The effect of complex water matrices on NAP degradation was evaluated, showing that sulfur-iron material-enhanced techniques had a wide pH application range and had great tolerance to inorganic ions and humic acid. Moreover, NAP degradation intermediates and their toxicity were elucidated. Finally, the obvious removal of various pollutants in sulfur-iron material-enhanced systems demonstrated that these technologies could be used to remediate organic-polluted groundwater.

Keywords: naphthalene; sulfur-iron materials; enhancement mechanism; reactive oxygen species; groundwater remediation

Academic Editor: Alexandre T. Paulino

Received: 12 March 2026
Revised: 3 April 2026
Accepted: 8 April 2026
Published: 11 April 2026

1. Introduction

Recently, the problem of remaining contaminated sites has been increasingly exposed with the relocation of enterprises, and efficient and rapid remediation methods are urgently needed to solve the problem. The research and implementation of advanced oxidation processes (AOPs) have received special attention due to their efficient performance on pollutant degradation and mineralization [1,2]. Some reactive oxygen species (ROS), such as hydroxyl radical (HO•, E^0 = 2.8 V) and sulfate radical (SO_4^-•, E^0 = 2.5~3.1 V), can be generated in AOPs, and they can rapidly react with organic compounds through addition, ring-opening, etc. [3,4]. The conventional Fenton process is one kind of AOPs, and HO•

is the major ROS in the Fenton process, which can degrade various organic compounds non-selectively and produce intermediate products [2,5].

As is well known, the obvious drawbacks of the conventional Fenton process are as follows. On the one hand, dissolved Fe(II) is easily precipitated and quickly consumed in a short period of time; thus, the sustaining provision of Fe(II) is indispensable for promoting the degradation of pollutants in the Fenton process. On the other hand, the Fenton reaction is extremely demanding on pH value, and an acidic condition (pH = 3) is always needed for the reaction [6]. To overcome these problems, sulfur-iron materials (such as sulfide-modified nanoscale zerovalent iron (S-nZVI), ferrous sulfide (FeS), and pyrite (FeS_2)) have been used as a stimulant for oxidant activation and as a enhancer for pollutant removal in AOPs due to the existence of the electron shuttle, sustainable release of Fe(II), Fe(II) regeneration by sulfur species, and resistance to a high value of pH [7–9].

Sulfidation refers to the reduction of iron salt by borohydrides and dithionites through the one-pot method, forming a mixture of S^{2-}, S_2^{2-}, poly S^{2-}, SO_3^{2-}, and SO_4^{2-} on the surface of nanoscale zerovalent iron (nZVI), and sulfur-iron species (such as FeS and FeS_2) can be formed simultaneously [10,11]. The main mechanisms of S-nZVI involved in the reaction process are as follows. On the one hand, these sulfur species can slow down the reaction between Fe(0) and O_2 by forming a core–shell structure, retarding the passivation of the material. On the other hand, these sulfur species as reductants can reduce the surface Fe(III) to Fe(II) by accelerating the electron shuttle [12]. Therefore, the introduction of S-nZVI in AOPs can improve the removal performance of various pollutants [9,13]. In addition, some literature has reported that heavy metals (such as Sb(III) and As(III)) could be effectively removed by S-nZVI directly due to its great reductivity [14,15].

In addition, as the main component of mackinawite, FeS has received extensive attention in pollutant removal, and it is involved in contaminant degradation in three ways. Firstly, the homogeneous reaction can be triggered by Fe(II) released from solid FeS in aqueous solution in acidic conditions according to Equation (1), and ROS can be produced by activating the oxidant with Fe(II) [16]. Secondly, the surface-active sites of FeS can contribute to the oxidation of pollutants, and the number of available sites increases with the increase in FeS dosage [17]. Thirdly, the reductive sulfur species in FeS can promote the reduction in Fe(III) and the regeneration of Fe(II), accelerating the activation of oxidants and the removal of pollutants [7]. Chen et al. (2015) found that 2,4-dichlorophenoxyacetic acid could be effectively removed in the H_2O_2/FeS system, and HO• was the dominant ROS for the pollutant removal [17].

$$FeS + 2H^+ \rightarrow Fe(II) + H_2S \quad (1)$$

Pyrite is the most abundant iron sulfide mineral in the crust of Earth, and FeS_2 is the main ingredient of natural pyrite [18]. The reaction mechanisms of FeS_2 involved in AOPs are as follows. On the one hand, HO• and H_2O_2 can be generated simultaneously in the presence of FeS_2 in aqueous solution according to Equations (2) and (3), and this process can be accelerated with the existence of oxygen (Equations (4)–(6)) [19,20]. On the other hand, H^+ can be generated in the oxidation process (Equation (4)), resulting in the rapid Fe(II) leaching from FeS_2 and the efficient activation of the oxidant. However, pollutant removal is limited in the presence of FeS_2 due to the deficient H_2O_2 production induced by FeS_2 [20]. Pollutants can be effectively degraded with the addition of exogenous H_2O_2. Bae et al. (2013) found that diclofenac could be completely degraded within 120 s in the H_2O_2/FeS_2 system. This was ascribed to the lower pH value caused by the presence of FeS_2 and the sustained dissolution of Fe(II) from FeS_2 [21].

$$H_2O_{(ads)} + Fe(III)_{(pyrite)} \rightarrow HO\bullet + Fe(II)_{(pyrite)} + H^+ \quad (2)$$

$$HO\bullet + HO\bullet \rightarrow H_2O_2 \quad (3)$$

$$2FeS_2 + 7O_2 + 2H_2O \rightarrow 2Fe(II) + 4SO_4^{2-} + 4H^+ \quad (4)$$

$$Fe(II) + O_2 \rightarrow Fe(III) + O_2^{-}\bullet \quad (5)$$

$$Fe(II) + 2H_2O + O_2^{-}\bullet \rightarrow H_2O_2 + Fe(III) + 2OH^- \quad (6)$$

Polycyclic aromatic hydrocarbons (PAHs) have been frequently found in contaminated sites, and it is urgent to remove them by efficient techniques [22]. However, the above three sulfur-iron materials (S-nZVI, FeS, and FeS_2) as the enhancers to remove PAHs in Fenton-like processes have not been reported yet. In this work, naphthalene (NAP) was selected as the representative PAHs, and the removal of NAP in the H_2O_2/Fe(II) process enhanced by S-nZVI, FeS, and FeS_2 was investigated. The aims of this work are to: (1) compare the removal performance of NAP in various systems enhanced by different sulfur-iron materials and elucidate the enhancement mechanism of different sulfur-iron materials in Fenton-like process; (2) illuminate the degradation mechanism of NAP and determine the major ROS for NAP removal in various systems; (3) explore the effect of different water matrixes on NAP removal and evaluate the effectiveness of Fenton-like systems enhanced by different sulfur-iron materials on NAP removal in actual groundwater; (4) reveal the NAP degradation intermediates and pathways in sulfur-iron material-enhanced systems; and (5) assess the applicability of these techniques in the removal of other pollutants.

2. Materials and Methods

2.1. Materials

H_2O_2 (30% wt) was acquired from Yonghua Chemical Co., Ltd. (Shanghai, China). S-nZVI (99.0%, ω(S) = 2%) was purchased from Shanghai Chaowei Nanotechnology Co., Ltd. (Shanghai, China). FeS (99.0%) was provided by Shanghai Macklin Biochemical Co., Ltd. (Shanghai, China). FeS_2 (95.0%) was supplied by Shanghai Pumai Biotechnology Co., Ltd. (Shanghai, China). The details of other chemicals used in this work are available in Text S1. The major parameters of the actual groundwater are provided in Table S1.

2.2. Experimental Procedures

NAP degradation experiments were performed in 250 mL reactors with the initial NAP concentration of 0.1 mM. The reaction was started when Fe(II), sulfur-iron materials (S-nZVI, FeS, and FeS_2), and H_2O_2 were added in sequence. At the given time, the sample was mixed with the same amount of methanol for quenching the reaction and then filtered for further determination of concentration by high-performance liquid chromatography (HPLC). All experiments were carried out in duplicate, and the data were shown in mean values.

2.3. Analytical Methods

The detailed analytical method for NAP by HPLC was provided in Text S2. The concentrations of H_2O_2 and Fe were detected by titanium sulfate spectrophotometry and 1,10-phenanthroline spectrophotometry, respectively [23,24]. The solution pH and dissolved oxygen (DO) were determined by a pH meter (FE28, Mettler-Toledo, Columbus, OH, USA) and a DO meter (JPB-607A, Shanghai Instrument & Electrical Scientific Instrument Co., Ltd., Shanghai, China), respectively. The specific analytical methods for NAP degradation intermediates and the parameters of actual groundwater were supplied in Text S2.

3. Results and Discussion

3.1. NAP Degradation Performance in Various Systems

The degradation performance of NAP in Fenton-like processes coupled with different sulfur-iron materials (S-nZVI, FeS, and FeS_2) was investigated, and the initial concentrations of H_2O_2, Fe(II), S-nZVI, FeS, FeS_2, and NAP were set as 0.5 mM, 0.3 mM, 0.03 g L^{-1}, 0.1 g L^{-1}, 1 g L^{-1}, and 0.1 mM, respectively. The initial reaction pH was not pre-adjusted (initial pH = 5.71). As shown in Figure S1, NAP could not be effectively degraded, and the removal was less than 7% within 120 min in the individual existence of H_2O_2, Fe(II), S-nZVI, FeS, and FeS_2, respectively. Without the addition of Fe(II), 5.1%, 5.7%, and 64.5% of NAP were removed in H_2O_2 oxidation processes activated by S-nZVI, FeS, and FeS_2, respectively. The above phenomenon can be explained as follows. Firstly, H_2O_2 could not be efficiently activated by these sulfur-iron materials (S-nZVI, FeS, and FeS_2), and the solubility of sulfur-iron materials was poor, resulting in the insignificant leaching of Fe(II); thus, ROS could not be generated along with the activation of H_2O_2, and NAP degradation was limited without Fe(II) addition [25]. However, FeS_2 could react with O_2 to form Fe(II) and H^+ in aqueous solution (Equation (4)), accelerating the FeS_2 dissolution; hence, NAP was removed continually in the H_2O_2/FeS_2 system. Moreover, H_2S could be generated according to Equation (1), but an unpleasant odor was not found in this work; this might be due to the small usage of FeS and the little production of H_2S. Moreover, the generated H_2S is soluble in water to form hydrosulfuric acid.

As illustrated in Figure 1, 56.4% removal of NAP was obtained in the H_2O_2/Fe(II) system within 120 min. Notably, NAP was removed rapidly within 1 min, but NAP could not be obviously degraded in the subsequent reaction time, showing that NAP could not be continuously and efficiently degraded in the traditional Fenton process. However, with the addition of S-nZVI, FeS, and FeS_2, the degradation efficiency of NAP was enhanced to 88.6%, 83.0%, and 89.1%, respectively, indicating that sulfur-iron materials could promote the production of ROS and the removal of NAP. Moreover, NAP degradation in these processes followed the pseudo-second-order kinetic model, and the kinetic results are shown in Table 1. The kinetic constant (k) of NAP degradation increased from 0.0340 mM^{-1} min^{-1} in the H_2O_2/Fe(II) process to 0.5792 mM^{-1} min^{-1}, 0.3445 mM^{-1} min^{-1}, and 0.5454 mM^{-1} min^{-1} in H_2O_2/Fe(II)/S-nZVI, H_2O_2/Fe(II)/FeS, and H_2O_2/Fe(II)/FeS_2 processes, respectively. In other words, k increased by 16, 9, and 15 times when three sulfur-iron materials were introduced, confirming the important role of sulfur-iron materials in NAP removal. These results can be clarified in the following two ways. Firstly, Fe(II) was continuously released from sulfur-iron materials during the reaction, which could promote the homogeneous reaction and the degradation of NAP [26]. Secondly, Fe(III) produced in the oxidation processes could be reduced to Fe(II) through reductive sulfur species, which could participate in the activation of oxidants and accelerate the production of ROS, further promoting the removal of NAP.

Moreover, the influence of various chemicals (H_2O_2, Fe(II), and sulfur-iron materials) on NAP degradation was explored. The degradation of NAP could be promoted by appropriately increasing the reagent dosages, but excessive chemicals were not conducive to the degradation of NAP by scavenging the generated ROS (Figure S2). In a word, the optimal concertation of H_2O_2, Fe(II), S-nZVI, FeS, and FeS_2 were 0.5 mM, 0.3 mM, 0.03 g L^{-1}, 0.1 g L^{-1}, and 1 g L^{-1}, respectively. Notably, a smaller dosage of S-nZVI was needed to achieve the ideal removal of NAP (>80%) among the three sulfur-iron materials, which was attributed to the reactivity of S-nZVI and the synergistic effect between S and Fe(0) [27].

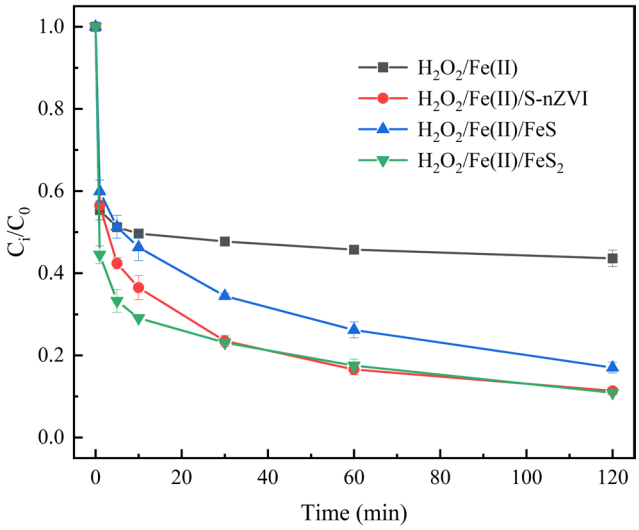

Figure 1. NAP degradation performance in different systems. ($[H_2O_2]_0$ = 0.5 mM, $[Fe(II)]_0$ = 0.3 mM, $[S\text{-}nZVI]_0$ = 0.03 g L^{-1}, $[FeS]_0$ = 0.1 g L^{-1}, $[FeS_2]_0$ = 1.0 g L^{-1}, $[NAP]_0$ = 0.1 mM).

Table 1. Pseudo-second-order kinetics of NAP degradation in various systems.

Processes	k (mM^{-1} min^{-1})	R^2
H_2O_2/Fe(II)	0.0340	0.8176
H_2O_2/Fe(II)/S-nZVI	0.5792	0.9837
H_2O_2/Fe(II)/FeS	0.3445	0.9975
H_2O_2/Fe(II)/FeS_2	0.5454	0.9905

3.2. Insights into the Enhancement Mechanism of Sulfur-Iron Materials

3.2.1. The Variation in Fe and H_2O_2 Concentrations

To explore the enhancement mechanism of S-nZVI, FeS, and FeS_2 on NAP degradation in Fenton-like systems, the concentrations of Fe(II) and total Fe in various systems were determined. The initial concentrations of H_2O_2, Fe(II), S-nZVI, FeS, FeS_2, and NAP were controlled at 0.5 mM, 0.3 mM, 0.03 g L^{-1}, 0.1 g L^{-1}, 1 g L^{-1}, and 0.1 mM, respectively.

As shown in Figure 2, the concentration of Fe(II) rapidly decreased from 0.3 mM to about 0.04 mM within 1 min in both H_2O_2/Fe(II) and H_2O_2/Fe(II)/sulfur-iron materials systems, demonstrating the rapid involvement of Fe(II) in the reaction of H_2O_2 activation. In the subsequent reaction from 1 min to 120 min, Fe(II) was almost exhausted and maintained at 0.004 mM in the H_2O_2/Fe(II) process, which explained the rapid degradation of NAP within 1 min and the unobvious removal in the subsequent time. In the other three sulfur-iron material-enhanced systems, the Fe(II) concentration was more than 0.010 mM within 120 min due to the sustained release of Fe(II) from sulfur-iron materials, which was conducive to the continuous activation of oxidants and the production of ROS. As for the variation in total Fe concentration, the amount of total Fe in the H_2O_2/Fe(II) system decreased from 0.3 mM to 0.038 mM within 120 min, because dissolved iron ions were transferred to iron precipitation during the reaction. However, in S-nZVI, FeS, and FeS_2-enhanced processes, the concentrations of total Fe after the reaction were 0.067 mM, 0.067 mM, and 0.096 mM, respectively, which were much greater than that (0.038 mM) in the system without enhancement. The above phenomenon could be expounded as follows. On the one hand, dissolved iron ions could be released continuously from the sulfur-iron materials during the reaction. On the other hand, S^0, S^{2-}, and S_2^{2-} in S-nZVI, FeS, and FeS_2 could reduce Fe(III) generated in these systems (Equations (7)–(9)), regenerate Fe(II), and slow down the precipitation of Fe(III). In addition, Fe(III) could also

be reduced by Fe(0) in S-nZVI. In conclusion, three sulfur-iron materials (S-nZVI, FeS, and FeS_2) could promote NAP removal by releasing Fe(II) and reducing Fe(III).

$$6Fe(III) + S^0 + 4H_2O \rightarrow 6Fe(II) + SO_4^{2-} + 8H^+ \quad (7)$$

$$8Fe(III) + S^{2-} + 4H_2O \rightarrow 8Fe(II) + SO_4^{2-} + 8H^+ \quad (8)$$

$$14Fe(III) + S_2^{2-} + 8H_2O \rightarrow 14Fe(II) + 2SO_4^{2-} + 16H^+ \quad (9)$$

Moreover, the consumption of H_2O_2 in different systems was explored, and the results are illustrated in Figure 2c. In the H_2O_2/Fe(II) process, the H_2O_2 amount decreased dramatically from 0.5 mM to 0.371 mM within 1 min, then decreased slowly during the subsequent reaction from 1 min to 120 min, and finally maintained at 0.345 mM, which was a similar trend to the variation of iron concentration. In three sulfur-iron material-enhanced systems, H_2O_2 was gradually consumed during the whole reaction, and the concentrations decreased from 0.5 mM to 0.035 mM, 0.065 mM, and 0.098 mM within 120 min in H_2O_2/Fe(II)/S-nZVI, H_2O_2/Fe(II)/FeS, and H_2O_2/Fe(II)/FeS_2 systems, respectively. Notably, the utilization efficiency of H_2O_2 increased from 31.0% in the H_2O_2/Fe(II) process to 93.0%, 87.0%, and 80.3% with the addition of S-nZVI, FeS, and FeS_2, respectively, demonstrating that sulfur-iron materials could facilitate the Fe(II)/Fe(III) circulation and accelerate the activation of H_2O_2.

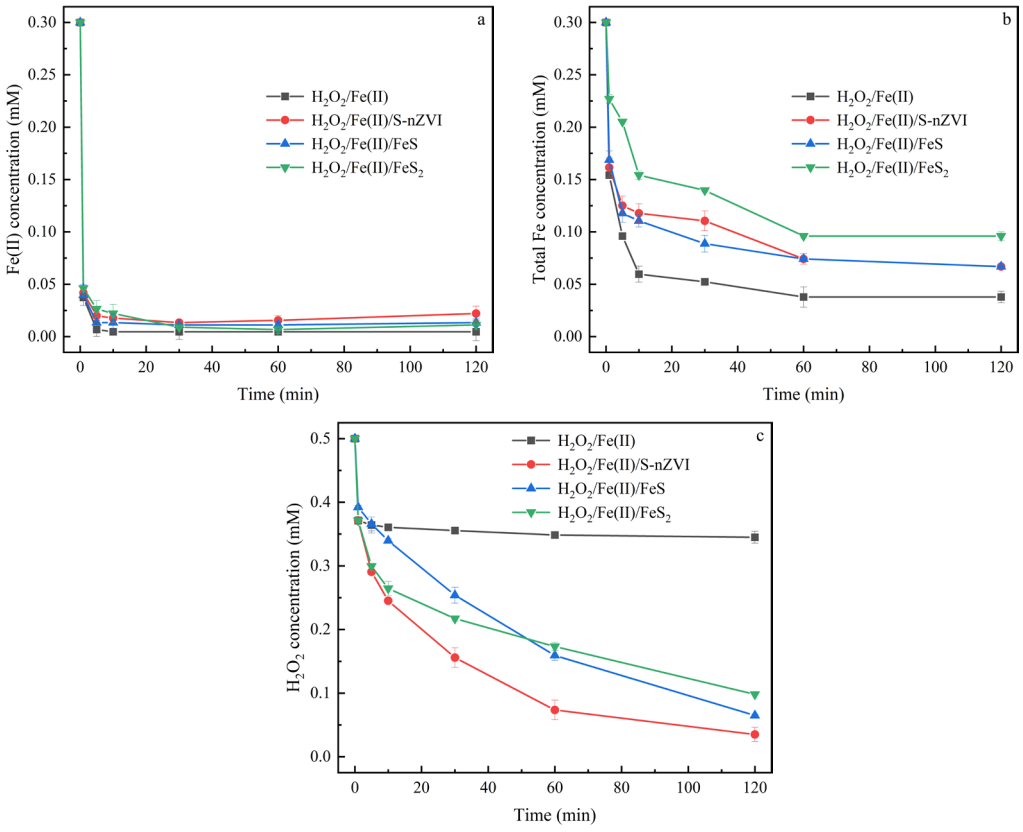

Figure 2. The variation of (**a**) Fe(II), (**b**) total Fe, and (**c**) H_2O_2 concentrations in different systems. ($[H_2O_2]_0$ = 0.5 mM, $[Fe(II)]_0$ = 0.3 mM, $[S\text{-}nZVI]_0$ = 0.03 g L^{-1}, $[FeS]_0$ = 0.1 g L^{-1}, $[FeS_2]_0$ = 1.0 g L^{-1}, $[NAP]_0$ = 0.1 mM).

3.2.2. The Variation in HO• Concentration

Benzoic acid (BA) was used as the capture of HO• to quantitatively analyze the concentration of generated HO•. *p*-Hydroxybenzoic acid (*p*-HBA) was the characteristic product of the reaction between BA and HO•, and there is a clear conversion coefficient

(5.87) between *p*-HBA and HO• [28]. Therefore, the amount of HO• produced in aqueous solution can be quantitatively determined indirectly by measuring the concentration of *p*-HBA. As shown in Figure 3, the amount of HO• accumulated within 120 min in the H_2O_2/Fe(II) system was 155.0 μM. Notably, the concentrations of HO• increased to 200.8 μM, 195.7 μM, and 218.0 μM with the addition of S-nZVI, FeS, and FeS_2, respectively, confirming that the presence of sulfur-iron materials could promote the ROS production and NAP removal. The presence of sulfur-iron materials could accelerate the circulation of Fe(II)/Fe(III), achieving the aim of efficient activation of oxidant and production of ROS.

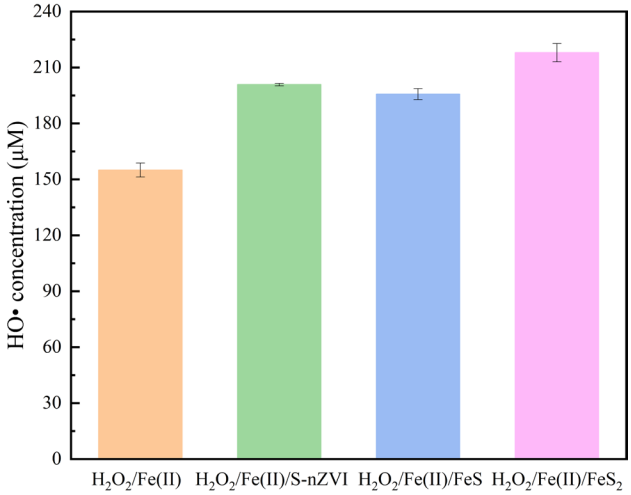

Figure 3. The accumulated concentration of HO• in different systems. ($[H_2O_2]_0$ = 0.5 mM, $[Fe(II)]_0$ = 0.3 mM, $[S\text{-}nZVI]_0$ = 0.03 g L^{-1}, $[FeS]_0$ = 0.1 g L^{-1}, $[FeS_2]_0$ = 1.0 g L^{-1}).

3.3. The Degradation Mechanism of NAP in Sulfur-Iron Material-Enhanced Systems

Reportedly, HO• and superoxide radical (O_2^-•) are the main ROS generated in the Fenton-like process [29]. In this work, to investigate the ROS produced in sulfur-iron material-enhanced systems, electron paramagnetic resonance (EPR) was employed, and 5,5-dimethyl-1-oxypyrrolidine (DMPO) was used as the ROS capture. The initial concentrations of H_2O_2, Fe(II), S-nZVI, FeS, and FeS_2 were controlled at 0.5 mM, 0.3 mM, 0.03 g L^{-1}, 0.1 g L^{-1}, and 1 g L^{-1}, respectively. As shown in Figure 4, the signals of DMPO-HO• were all found in H_2O_2/Fe(II)/S-nZVI, H_2O_2/Fe(II)/FeS, and H_2O_2/Fe(II)/FeS_2 processes, confirming the generation of HO• in these three systems. However, the characteristic peaks of the products generated by the reaction between DMPO and O_2^-• were not observed by EPR in the above three systems, which might be due to the instability of O_2^-• in aqueous solution [30].

Moreover, the scavenging tests were conducted to confirm the contribution of diverse ROS to NAP removal and determine the dominant ROS. Tertiary butanol (TBA) and chloroform (CF) were used as the scavengers of HO• and O_2^-• due to their great reactivity with the specific ROS, respectively [31,32]. As illustrated in Figure 5, 88.6%, 83.0%, and 89.1% of NAP could be removed in H_2O_2/Fe(II)/S-nZVI, H_2O_2/Fe(II)/FeS, and H_2O_2/Fe(II)/FeS_2 processes without the presence of scavengers, while NAP removal decreased to 9.9%, 9.0%, and 7.4% with the addition of 100 mM TBA, respectively, demonstrating that HO• was the dominated ROS in these three systems and contributed tremendously to NAP degradation. Notably, with the existence of 50 mM CF, NAP degradation was slightly restrained in these three processes, and the removal decreased to 69.8%, 77.9%, and 85.8%, respectively, and the result indicated that O_2^-• also participated in NAP degradation in sulfur-iron material-enhanced systems, especially in the H_2O_2/Fe(II)/S-nZVI system.

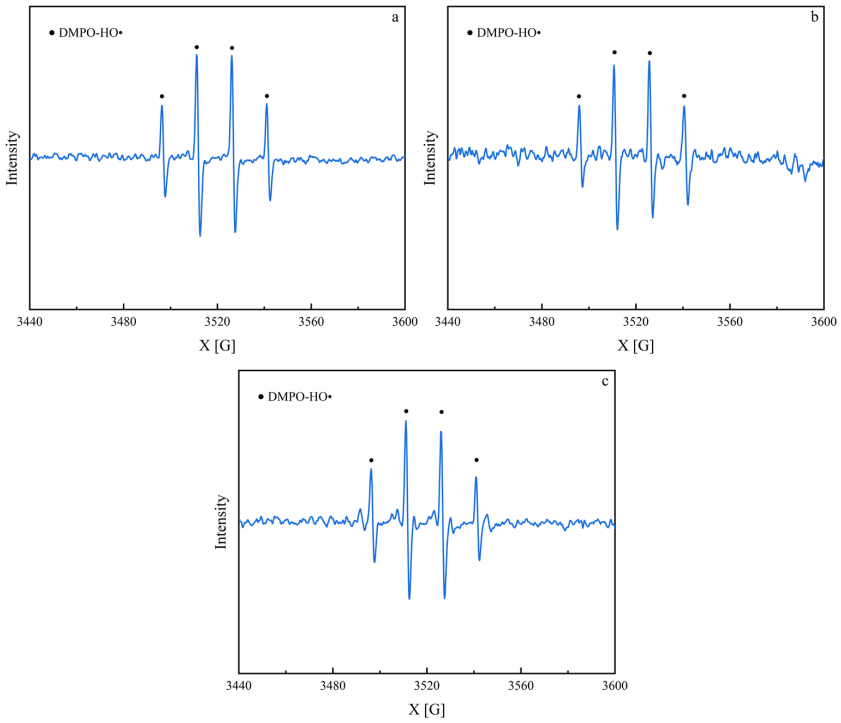

Figure 4. EPR detection in (**a**) H_2O_2/Fe(II)/S-nZVI, (**b**) H_2O_2/Fe(II)/FeS, and (**c**) H_2O_2/Fe(II)/FeS_2 systems. ($[H_2O_2]_0$ = 0.5 mM, $[Fe(II)]_0$ = 0.3 mM, $[S\text{-}nZVI]_0$ = 0.03 g L^{-1}, $[FeS]_0$ = 0.1 g L^{-1}, $[FeS_2]_0$ = 1.0 g L^{-1}).

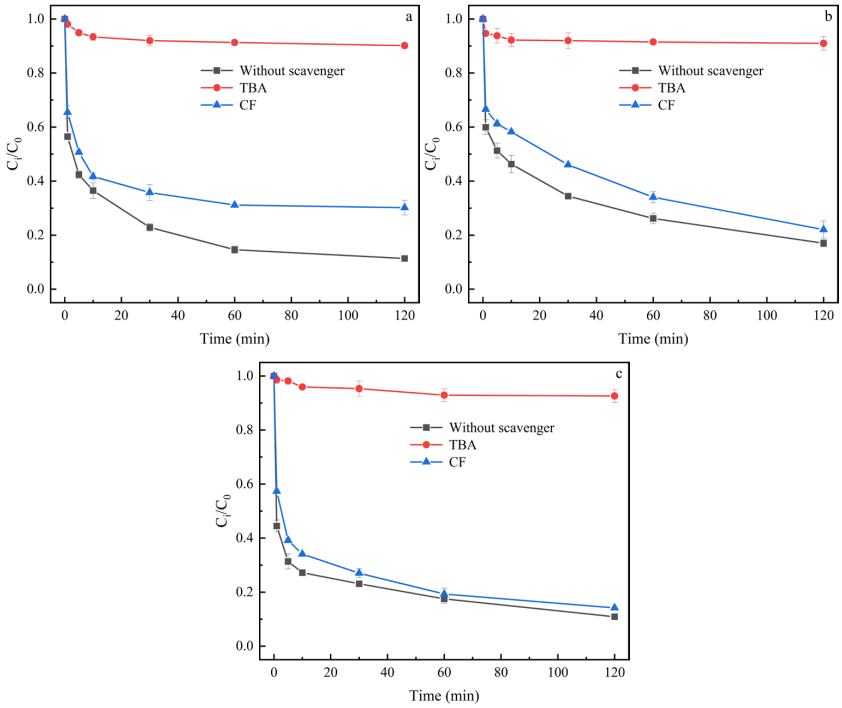

Figure 5. The effect of different scavengers on NAP removal in (**a**) H_2O_2/Fe(II)/S-nZVI, (**b**) H_2O_2/Fe(II)/FeS, and (**c**) H_2O_2/Fe(II)/FeS_2 systems. ($[H_2O_2]_0$ = 0.5 mM, $[Fe(II)]_0$ = 0.3 mM, $[S\text{-}nZVI]_0$ = 0.03 g L^{-1}, $[FeS]_0$ = 0.1 g L^{-1}, $[FeS_2]_0$ = 1.0 g L^{-1}, $[NAP]_0$ = 0.1 mM, $[TBA]_0$ = 100 mM, $[CF]_0$ = 50 mM).

3.4. The Influence of Water Matrices on NAP Degradation in Sulfur-Iron Material-Enhanced Systems

To assess the effectiveness of sulfur-iron materials-nhanced systems on NAP degradation in complex water matrices, the effect of solution pH was first explored. The initial

dosages of H_2O_2, Fe(II), S-nZVI, FeS, FeS_2, and NAP were set as 0.5 mM, 0.3 mM, 0.03 g L^{-1}, 0.1 g L^{-1}, 1 g L^{-1}, and 0.1 mM, respectively. As shown in Figure S3, NAP removal changed slightly and was more than 80% with the initial solution pH increasing from 3 to 9 in the H_2O_2/Fe(II)/S-nZVI system, showing that the S-nZVI-enhanced process could degrade NAP effectively with the value of initial pH from 3 to 9. Similar experimental results were observed in H_2O_2/Fe(II)/FeS and H_2O_2/Fe(II)/FeS_2 processes, namely, NAP could be effectively removed in both systems when the solution pH was 3 to 9, demonstrating that the pH application range of sulfur-iron material-enhanced systems was wide.

Secondly, four common inorganic ions (Cl^-, HCO_3^-, SO_4^{2-}, and NO_3^-) were selected as the representatives presented in actual groundwater, and the effect of inorganic ions was explored. The presence of different concentrations of Cl^- exerted an insignificant influence on NAP removal and solution pH variation (Figure S4 and Table S2). This can be expounded in the following ways. On the one hand, Cl^- can scavenge HO• generated in aqueous solution. On the other hand, some reactive chlorine species (such as chloride radical and dichloride radical) can be generated by the chain reaction between Cl^- and HO•, which may contribute to NAP removal [33]. However, with the presence of HCO_3^-, NAP removal was obviously inhibited in sulfur-iron material-enhanced systems, and the inhibitory effect was more obvious with the augmentation of HCO_3^- concentration (Figure S4). This is because that the existence of HCO_3^- could increase the pH value, with the existence of 10 mM HCO_3^-, the value of solution pH increased from 5.71 to 8.63, 8.55, and 8.56 in H_2O_2/Fe(II)/S-nZVI, H_2O_2/Fe(II)/FeS, and H_2O_2/Fe(II)/FeS_2 system, respectively (Table S2). In addition, the presence of HCO_3^- could enhance the buffering of the solution and scavenge HO•, thus inhibiting the degradation of NAP [27]. In the presence of various concentrations (1~100 mM) of SO_4^{2-} and NO_3^-, NAP removal changed little; hence, the effect of them on NAP degradation could be omitted in this work (Figure S4).

Thirdly, humic acid (HA) was chosen as the representative of natural organic matter in groundwater, and the effect on NAP removal is shown in Figure S5. With the concentration of HA increasing from 0 to 50 mM, NAP removal changed insignificantly in H_2O_2/Fe(II)/S-nZVI, H_2O_2/Fe(II)/FeS, and H_2O_2/Fe(II)/FeS_2 processes, demonstrating that sulfur-iron material-enhanced systems had a great tolerance to HA. Though the presence of HA could compete with the target pollutant for the generated ROS, the precipitation of dissolved iron ions could be slowed down through HA chelation [34]. Thus, the negative effects of ROS consumption caused by HA could be offset through its chelation of dissolved iron ions and promoting the generation of ROS.

Moreover, dissolved oxygen (DO) is also an important parameter in actual groundwater. Thus, three concentrations (0 mg L^{-1}, 4 mg L^{-1}, and 8.8 mg L^{-1} (unadjusted)) of DO were controlled by nitrogen blowing to investigate the influence of DO on NAP degradation. As seen in Figure 6, when the DO concentration was unadjusted (8.8 mg L^{-1}), NAP removal was 88.6%, 83.0%, and 89.1% in H_2O_2/Fe(II)/S-nZVI, H_2O_2/Fe(II)/FeS, and H_2O_2/Fe(II)/FeS_2 processes, respectively. With the amount of DO adjusted to 4 mg L^{-1}, NAP removal decreased to 61.5%, 72.5%, and 68.4% in these three sulfur-iron material-enhanced systems, respectively. However, only 44.6%, 47.0%, and 45.9% of NAP could be removed when the concentration of DO was controlled at 0 mg L^{-1}. The above results showed that DO took part in the degradation of NAP. Our previous study also found that DO could be involved in the chain reaction of ROS and affect the production of ROS, thus inhibiting the removal of pollutants [35].

Finally, the degradation performance of NAP in actual groundwater in sulfur-iron material-enhanced systems was explored, and the results are shown in Figure 7. Only 10.7%, 8.5%, and 9.4% of NAP could be degraded in actual groundwater in H_2O_2/Fe(II)/S-nZVI, H_2O_2/Fe(II)/FeS, and H_2O_2/Fe(II)/FeS_2 processes, respectively, which were much lower

than the results in ultrapure water (88.6%, 83.0%, and 89.1%). This phenomenon can be clarified as follows. The actual groundwater was alkaline, had the property of buffering, and contained a lot of organic matter (TOC = 38.25 mg L^{-1}) and HCO_3^- (96.8 mg L^{-1}) (Table S1), which were not conducive to the degradation of NAP. Fortunately, when the chemical dosages were increased to 10 times, NAP removal increased to 76.5%, 73.6%, and 83.7% in these three sulfur-iron material-enhanced systems, respectively, demonstrating that sulfur-iron material-enhanced techniques can be applied to effectively remove NAP in polluted groundwater.

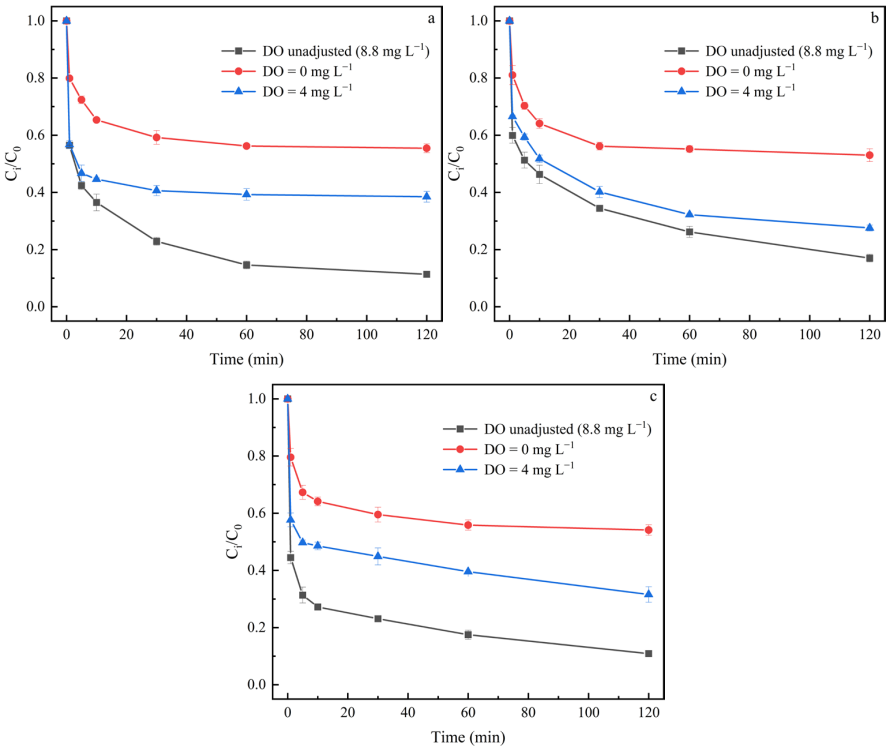

Figure 6. The effect of different DO concentrations on NAP removal in (**a**) H_2O_2/Fe(II)/S-nZVI, (**b**) H_2O_2/Fe(II)/FeS, and (**c**) H_2O_2/Fe(II)/FeS_2 systems. ($[H_2O_2]_0$ = 0.5 mM, $[Fe(II)]_0$ = 0.3 mM, $[S\text{-}nZVI]_0$ = 0.03 g L^{-1}, $[FeS]_0$ = 0.1 g L^{-1}, $[FeS_2]_0$ = 1.0 g L^{-1}, $[NAP]_0$ = 0.1 mM).

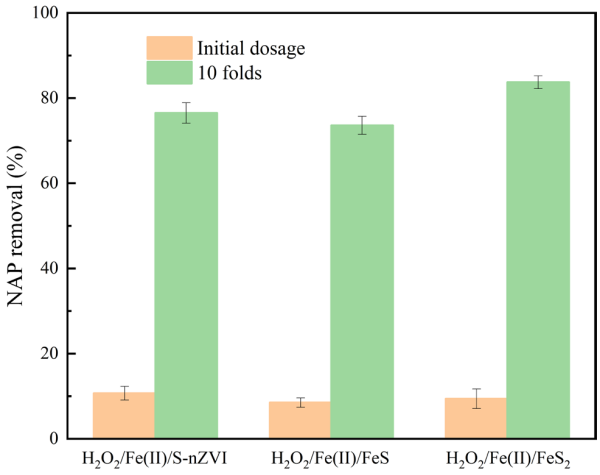

Figure 7. NAP degradation performance in actual groundwater in sulfur-iron material-enhanced systems. ($[NAP]_0$ = 0.1 mM).

3.5. Applicability of Sulfur-Iron Material-Enhanced Systems for Other Pollutants

To assess the wide applicability of sulfur-iron material-enhanced systems for the remediation of actual contaminated groundwater, different pollutants (trichloroethylene (TCE), perchloroethylene (PCE), phenanthrene (PHE), and fluoranthene (FLT)) were selected as the representatives of common contaminants in polluted groundwater to explore their degradation performance in sulfur-iron material-enhanced processes. As exhibited in Figure 8, 96.4%, 92.3%, and 97.6% of TCE could be removed in H_2O_2/Fe(II)/S-nZVI, H_2O_2/Fe(II)/FeS, and H_2O_2/Fe(II)/FeS_2 processes, respectively, and PCE removal could reach 95.9%, 91.4%, and 94.7% in these three systems. Notably, PHE and FLT could be fully removed within 120 min in sulfur-iron material-enhanced systems. The above results demonstrated that sulfur-iron material-enhanced systems in this work had a great performance on the removal of other pollutants and had broad prospects of application.

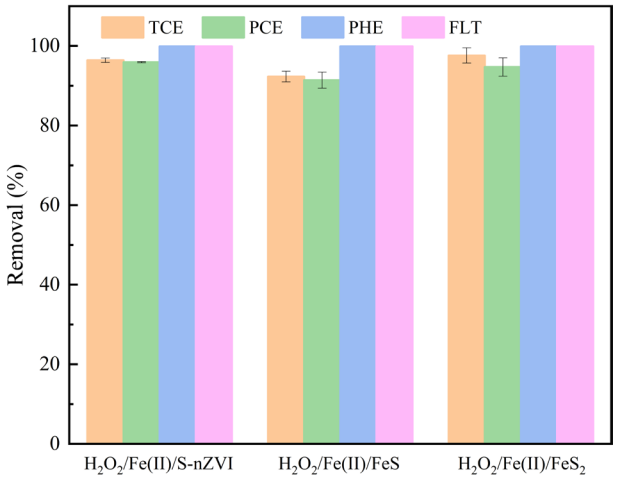

Figure 8. The degradation performance of various contaminants in sulfur-iron material-enhanced systems. ($[H_2O_2]_0$ = 0.5 mM, $[Fe(II)]_0$ = 0.3 mM, $[S\text{-}nZVI]_0$ = 0.03 g L^{-1}, $[FeS]_0$ = 0.1 g L^{-1}, $[FeS_2]_0$ = 1.0 g L^{-1}, $[TCE]_0 = [PCE]_0$ = 0.1 mM, $[PHE]_0$ = 5.6 μM, $[FLT]_0$ = 1.0 μM).

3.6. NAP Degradation Pathways and Intermediates Toxicity Estimation

NAP degradation intermediates in H_2O_2/Fe(II) processes coupled with sulfur-iron materials (S-nZVI, FeS, and FeS_2) were detected by LC-MS/MS. As illustrated in Table S3 and Figure S6, three NAP degradation intermediates (benzoic acid, phthalic anhydride, and 1,4-naphthalenediol) were all found in the above three oxidation processes.

According to the observations of LC-MS/MS, two possible degradation pathways of NAP were proposed (Figure 9). 1-Naphthol was discovered because of the addition of HO• on the NAP molecule, then 1,4-naphthalenediol was generated through hydroxylation, which was further converted to 1,4-naphthoquinone by tautomerism. In the meantime, two possible removal pathways could exist in the removal of 1,4-naphthoquinone. One was that benzaldehyde was produced from 1,4-naphthoquinone by hydroxylation and ring-opening, and it was transformed to benzoic acid through oxidation, resulting in the generation of phenol through the loss of CO_2 from benzoic acid. The other was that phthalic anhydride was generated by 1,4-naphthoquinone through oxidation, ring-opening, and loss of CO, and then it was transformed to phthalic acid through hydrolysis [36]. Finally, CO_2 and H_2O could be formed by these degradation intermediates through further oxidation.

The preliminary results of intermediate toxicity estimation by the Toxicity Estimation Software Tool (version 5.1.2) are shown in Figure 10 and Table S4. Except for 1,4-naphthalenediol, the LC_{50} (chemical concentration that kills half of the fathead minnow after 96 h) values of the other two intermediates (benzoic acid and phthalic anhydride) were greater than that of NAP (7.71 mg L^{-1}), demonstrating their lower acute toxicity.

Notably, all the intermediates showed lower values of the bioaccumulation factors than NAP. Except for 1,4-naphthalenediol, benzoic acid, and phthalic anhydride were classified as "developmental non-toxicant", and their developmental toxicity factor was lower than 0.5. Moreover, only phthalic anhydride and 1,4-naphthalenediol showed greater mutagenicity, but they were still categorized into "mutagenicity negative". In conclusion, although 1,4-naphthalenediol, with greater toxicity, was produced, it could be transformed to the less toxic intermediates (benzoic acid and phthalic anhydride) through oxidation during the degradation of NAP.

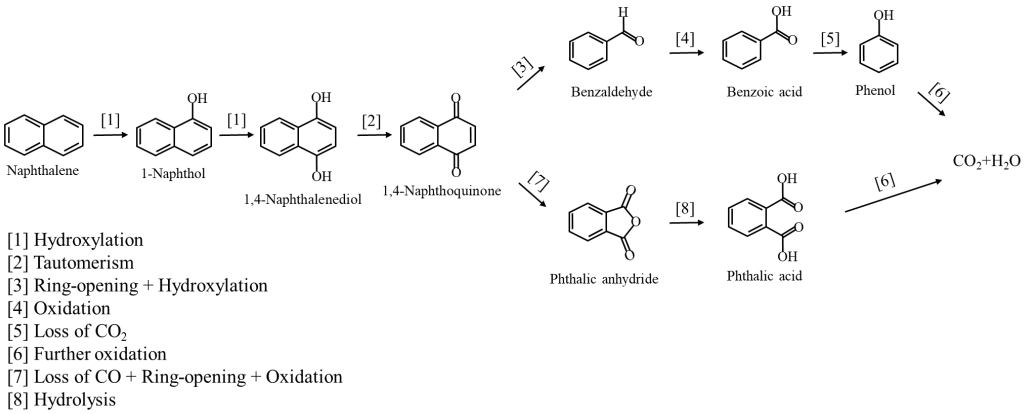

Figure 9. Proposed degradation pathway of NAP.

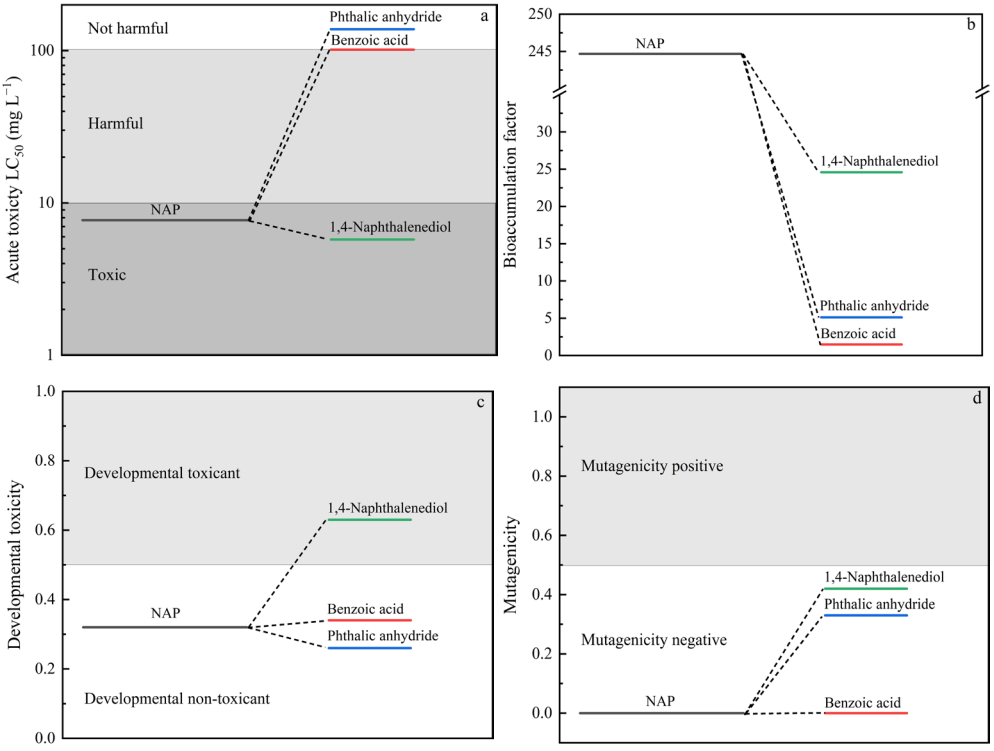

Figure 10. Toxicity evaluation, (**a**) acute toxicity, (**b**) bioaccumulation factor, (**c**) developmental toxicity, and (**d**) mutagenicity.

4. Conclusions

In this work, NAP degradation in Fenton-like processes enhanced by S-nZVI, FeS, and FeS_2 was investigated, and the enhancement performance and mechanism of these three sulfur-iron materials were revealed and compared. The results showed that only 56.4% of NAP was degraded in the H_2O_2/Fe(II) system, while NAP removal increased to 88.6%,

83.0%, and 89.1% with the addition of S-nZVI, FeS, and FeS_2, respectively, demonstrating that the existence of sulfur-iron materials could promote the removal of NAP. Based on the results of the variation in Fe concentration in the above systems, it can be concluded that the three sulfur-iron materials could all reduce Fe(III) produced in aqueous solution, regenerate Fe(II), and slow down the precipitation of dissolved iron. In addition, the addition of sulfur-iron materials could promote the generation of HO• in aqueous solution, thus enhancing the degradation of NAP. The results of scavenging tests indicated that HO• was the dominant ROS for NAP removal, while O_2^-• also contributed to the degradation of NAP. The effect of complex water matrices on NAP removal was evaluated, and the results showed that sulfur-iron material-enhanced techniques had a wide pH application range and great tolerance to inorganic ions and humic acid. Moreover, three degradation intermediates of NAP were found by LC-MS/MS in sulfur-iron material-enhanced processes, among which the acute toxicity of 1,4-naphthalenediol was stronger, while those of benzoic acid and phthalic anhydride were weaker. Two degradation pathways of NAP were proposed. Finally, according to the removal performance of other PAHs and chlorinated alkene (>90%), sulfur-iron material-enhanced processes could be suitable for the efficient restoration of complex polluted groundwater.

Supplementary Materials: The following supporting information can be downloaded at: https://www.mdpi.com/article/10.3390/w18080918/s1, Text S1. Materials. Text S2. Analytical methods. Figure S1. NAP degradation performance in different systems. Figure S2. The effect of (a) H_2O_2 ($[Fe(II)]_0$ = 0.3 mM, $[S\text{-}nZVI]_0$ = 0.03 g L^{-1}, $[FeS]_0$ = 0.1 g L^{-1}, $[FeS_2]_0$ = 1.0 g L^{-1}), (b) Fe(II) ($[H_2O_2]_0$ = 0.5 mM, $[S\text{-}nZVI]_0$ = 0.03 g L^{-1}, $[FeS]_0$ = 0.1 g L^{-1}, $[FeS_2]_0$ = 1.0 g L^{-1}), and (c) surfur-iron materials ($[H_2O_2]_0$ = 0.5 mM, $[Fe(II)]_0$ = 0.3 mM) dosages on NAP degradation in different systems. ($[NAP]_0$ = 0.1 mM). Figure S3. The effect of solution pH on NAP degradation in (a) H_2O_2/Fe(II)/S-nZVI, (b) H_2O_2/Fe(II)/FeS, and (c) H_2O_2/Fe(II)/FeS_2 systems. ($[H_2O_2]_0$ = 0.5 mM, $[Fe(II)]_0$ = 0.3 mM, $[S\text{-}nZVI]_0$ = 0.03 g L^{-1}, $[FeS]_0$ = 0.1 g L^{-1}, $[FeS_2]_0$ = 1.0 g L^{-1}, $[NAP]_0$ = 0.1 mM). Figure S4. The effect of different inorganic ions on NAP removal in (a) H_2O_2/Fe(II)/S-nZVI, (b) H_2O_2/Fe(II)/FeS, and (c) H_2O_2/Fe(II)/FeS_2 systems. ($[H_2O_2]_0$ = 0.5 mM, $[Fe(II)]_0$ = 0.3 mM, $[S\text{-}nZVI]_0$ = 0.03 g L^{-1}, $[FeS]_0$ = 0.1 g L^{-1}, $[FeS_2]_0$ = 1.0 g L^{-1}, $[NAP]_0$ = 0.1 mM). Figure S5. The effect of HA on NAP removal in (a) H_2O_2/Fe(II)/S-nZVI, (b) H_2O_2/Fe(II)/FeS, and (c) H_2O_2/Fe(II)/FeS_2 systems. ($[H_2O_2]_0$ = 0.5 mM, $[Fe(II)]_0$ = 0.3 mM, $[S\text{-}nZVI]_0$ = 0.03 g L^{-1}, $[FeS]_0$ = 0.1 g L^{-1}, $[FeS_2]_0$ = 1.0 g L^{-1}, $[NAP]_0$ = 0.1 mM). Figure S6. LC-MS/MS mass spectrums of NAP degradation intermediates. Table S1. The main characteristics of actual groundwater. Table S2. Parameter values in various systems. Table S3. The details of NAP degradation intermediates detected by LC-MS/MS in negative electrospray ionization mode. Table S4. The toxicological properties of NAP and intermediates.

Author Contributions: G.Z.: Conceptualization, Methodology, Software, Investigation, Data Curation, Writing—Original Draft. C.Z.: Formal analysis, Validation, Writing—Review and Editing. S.L.: Validation, Writing—Review and Editing. X.M.: Validation, Writing—Review and Editing, Supervision, Project administration, Funding acquisition. All authors have read and agreed to the published version of the manuscript.

Funding: This work was financially supported by the National Key R&D Program of China (2024YFC3713302), Zhejiang Provincial Postdoctoral Research Excellence Funding Program (ZJ2025168), and Special Project of Zhejiang Provincial Department of Science and Technology for Research Institutes (Research on Precision Diagnosis and Green Remediation Technology for Chlorinated Hydrocarbon Pollution in Groundwater).

Data Availability Statement: All data generated or analyzed during this study are included in this manuscript and Supplementary Materials.

Conflicts of Interest: The authors declare no conflicts of interest.

References

1. Preethi; Shanmugavel, S.; Kumar, G.; Yogalakshmi, K.; Gunasekaran, M.; Rajesh Banu, J. Recent progress in mineralization of emerging contaminants by advanced oxidation process: A review. *Environ. Pollut.* **2024**, *341*, 122842. [CrossRef] [PubMed]
2. Ziembowicz, S.; Kida, M. Limitations and future directions of application of the Fenton-like process in micropollutants degradation in water and wastewater treatment: A critical review. *Chemosphere* **2022**, *296*, 134041. [CrossRef] [PubMed]
3. Qu, R.; Li, C.; Liu, J.; Xiao, R.; Pan, X.; Zeng, X.; Wang, Z.; Wu, J. Hydroxyl radical based photocatalytic degradation of halogenated organic contaminants and paraffin on silica gel. *Environ. Sci. Technol.* **2018**, *52*, 7220–7229. [CrossRef] [PubMed]
4. Ye, C.; Ma, X.Y.; Deng, J.; Li, X.Y.; Li, Q.S.; Dietrich, A.M. Degradation of saccharin by UV/H_2O_2 and UV/PS processes: A comparative study. *Chemosphere* **2022**, *288*, 132337. [CrossRef]
5. Dai, H.; Luo, W.; Jin, L.; Deng, L.; Wang, Q.; Hu, J.; Singh, R. Degradation of chloroquine phosphate during UV/H_2O_2 process: Performance, kinetics, and degradation pathways. *J. Environ. Chem. Eng.* **2024**, *12*, 112493. [CrossRef]
6. Soufi, A.; Hajjaoui, H.; Boumya, W.; Elmouwahidi, A.; Baillón-García, E.; Abdennouri, M.; Barka, N. Recent trends in magnetic spinel ferrites and their composites as heterogeneous Fenton-like catalysts: A review. *J. Environ. Manag.* **2024**, *367*, 121971. [CrossRef]
7. Hong, Q.; Liu, C.; Wang, Z.; Li, R.; Liang, X.; Wang, Y.; Zhang, Y.; Song, Z.; Xiao, Z.; Cui, T.; et al. Electron transfer enhancing Fe(II)/Fe(III) cycle by sulfur and biochar in magnetic FeS@biochar to active peroxymonosulfate for 2,4-dichlorophenoxyacetic acid degradation. *Chem. Eng. J.* **2021**, *417*, 129238. [CrossRef]
8. Karim, A.; Jiao, Y.; Zhou, M.; Nidheesh, P. Iron-based persulfate activation process for environmental decontamination in water and soil. *Chemosphere* **2021**, *265*, 129057. [CrossRef]
9. Wu, J.; Zhao, J.; Hou, J.; Zeng, R.; Xing, B. Degradation of tetrabromobisphenol a by sulfidated nanoscale zerovalent iron in a dynamic two-step anoxic/oxic process. *Environ. Sci. Technol.* **2019**, *53*, 8105–8114. [CrossRef]
10. Su, Y.; Adeleye, A.; Keller, A.; Huang, Y.; Dai, C.; Zhou, X.; Zhang, Y. Magnetic sulfide-modified nanoscale zerovalent iron (S-nZVI) for dissolved metal ion removal. *Water Res.* **2015**, *74*, 47–57. [CrossRef]
11. Liu, Y.; Gao, J.; Wang, Q.; Chen, H.; Zhang, Y.; Fu, X. Efficient peroxymonosulfate activation by nanoscale zerovalent iron for removal of sulfadiazine and sulfadiazine resistance bacteria: Sulfidated modification or not. *J. Hazard. Mater.* **2024**, *469*, 133869. [CrossRef] [PubMed]
12. Yu, X.; Jin, X.; Li, M.; Yu, Y.; Zhu, M.; Tang, S.; Zhou, H.; Wang, K.; Dou, R.; Sun, J. Degradation mechanism of tetracycline using sulfidated nanoscale zerovalent iron driven peroxymonosulfate and metabolomic insights into environmental risk of intermediates products. *Chem. Eng. J.* **2022**, *430*, 133141. [CrossRef]
13. Su, Y.; Jassby, D.; Song, S.; Zhou, X.; Zhao, H.; Filip, J.; Petala, E.; Zhang, Y. Enhanced oxidative and adsorptive removal of diclofenac in heterogeneous Fenton-like reaction with sulfide modified nanoscale zerovalent iron. *Environ. Sci. Technol.* **2018**, *52*, 6466–6475. [CrossRef] [PubMed]
14. Liu, S.; Feng, H.; Tang, L.; Dong, H.; Wang, J.; Yu, J.; Feng, C.; Liu, Y.; Luo, T.; Ni, T. Removal of Sb(III) by sulfidated nanoscale zerovalent iron: The mechanism and impact of environmental conditions. *Sci. Total Environ.* **2020**, *736*, 139629. [CrossRef]
15. Zhao, J.; Su, A.; Tian, P.; Tang, X.; Collins, R.; He, F. Arsenic (III) removal by mechanochemically sulfidated microscale zero valent iron under anoxic and oxic conditions. *Water Res.* **2021**, *198*, 117132. [CrossRef]
16. Sun, Y.; Danish, M.; Ali, M.; Shan, A.; Li, M.; Lyu, Y.; Qiu, Z.; Sui, Q.; Zang, X.; Lyu, S. Trichloroethene degradation by nanoscale CaO_2 activated with Fe(II)/FeS: The role of FeS and the synergistic activation mechanism of Fe(II)/FeS. *Chem. Eng. J.* **2020**, *194*, 124830. [CrossRef]
17. Chen, H.; Zhang, Z.; Yang, Z.; Yang, Q.; Li, B.; Bai, Z. Heterogeneous Fenton-like catalytic degradation of 2,4-dichlorophenoxyacetic acid in water with Fes. *Chem. Eng. J.* **2015**, *273*, 481–489. [CrossRef]
18. Wang, C.; Sun, R.; Huang, R.; Cao, Y. A novel strategy for enhancing heterogeneous Fenton degradation of dye wastewater using natural pyrite: Kinetics and mechanism. *Chemosphere* **2021**, *272*, 129883. [CrossRef]
19. Chen, S.; Xiong, P.; Zhan, W.; Xiong, L. Degradation of ethylthionocarbamate by pyrite-activated persulfate. *Miner. Eng.* **2018**, *122*, 38–43. [CrossRef]
20. Wang, W.; Qu, Y.; Yang, B.; Liu, X.; Su, W. Lactate oxidation in pyrite suspension: A Fenton-like process in situ generating H_2O_2. *Chemosphere* **2012**, *86*, 376–382. [CrossRef]
21. Bae, S.; Kim, D.; Lee, W. Degradation of diclofenac by pyrite catalyzed Fenton oxidation. *Appl. Catal. B Environ.* **2013**, *134–135*, 93–102. [CrossRef]
22. Huang, J.; Zhu, B.; Song, D.; Wang, B.; Chen, L.; Lu, L.; Chen, Q.; Gai, L.; Zhai, C.; Chen, L.; et al. Synergistic photocatalysis for naphthalene (NAP) removal in seawater by S-scheme heterojunction Bi_2S_3/$CeVO_4$: Mechanistic investigation and degradation pathways. *Chem. Eng. J.* **2023**, *464*, 142784. [CrossRef]
23. Deadman, B.J.; Hellgardt, K.; Hii, K.K. A colorimetric method for rapid and selective quantification of peroxodisulfate, peroxomonosulfate and hydrogen peroxide. *React. Chem. Eng.* **2017**, *2*, 462–466. [CrossRef]

24. Harvey, A.E.; Smart, J.A.; Amis, E.S. Simultaneous spectrophotometric determination of iron(II) and total iron with 1,10-phenanthroline. *Anal. Chem.* **1955**, *27*, 26–29. [CrossRef]
25. Oh, S.Y.; Kang, S.G.; Kim, D.W.; Chiu, P.C. Degradation of 2,4-dinitrotoluene by persulfate activated with iron sulfides. *Chem. Eng. J.* **2011**, *172*, 641–646. [CrossRef]
26. Zhao, L.; Chen, Y.; Liu, Y.; Luo, C.; Wu, D. Enhanced degradation of chloramphenicol at alkaline conditions by S(-II) assisted heterogeneous Fenton-like reactions using pyrite. *Chemosphere* **2017**, *188*, 557–566. [CrossRef] [PubMed]
27. Wu, G.; Kong, W.; Gao, Y.; Kong, Y.; Dai, Z.; Dan, H.; Shang, Y.; Wang, S.; Yin, F.; Yue, Q.; et al. Removal of chloramphenicol by sulfide-modified nanoscale zero-valent iron activated persulfate: Performance, salt resistance, and reaction mechanisms. *Chemosphere* **2022**, *286*, 131876. [CrossRef] [PubMed]
28. Zhou, X.; Mopper, K. Determination of photochemically produced hydroxyl radicals in seawater and freshwater. *Mar. Chem.* **1990**, *30*, 71–88. [CrossRef]
29. Zhang, C.; Ding, N.; Pan, Y.; Fu, L.; Zhang, Y. The degradation pathways of contaminants by reactive oxygen species generated in the Fenton/Fenton-like systems. *Chin. Chem. Lett.* **2024**, *35*, 109579. [CrossRef]
30. Fang, G.D.; Dionysiou, D.D.; Al-Abed, S.R.; Zhou, D.M. Superoxide radical driving the activation of persulfate by magnetite nanoparticles: Implications for the degradation of PCBs. *Appl. Catal. B Environ.* **2013**, *129*, 325–332. [CrossRef]
31. Buxton, G.V.; Greenstock, C.L.; Helman, W.P.; Ross, A.B. Critical review of rate constants for reactions of hydrated electrons, hydrogen atoms and hydroxyl radicals (OH/O) in aqueous solution. *J. Phys. Chem. Ref. Data* **1988**, *17*, 513–886. [CrossRef]
32. Oyekunle, D.; Li, D.; Zheng, L.; Luo, F.; Wang, S.; Chen, Z. Enhanced degradation of organic compounds through the interfacial transfer of electrons in the presence of phosphate and Nitrogen-cobalt doped graphitic carbon. *J. Colloid Interface Sci.* **2022**, *607*, 1641–1650. [CrossRef]
33. Yang, Y.; Cao, Y.; Jiang, J.; Lu, X.L.; Ma, J.; Pang, S.Y.; Li, J.; Liu, Y.Z.; Zhou, Y.; Guan, C.T. Comparative study on degradation of propranolol and formation of oxidation products by UV/H_2O_2 and UV/persulfate (PDS). *Water Res.* **2019**, *149*, 543–552. [CrossRef]
34. Georgi, A.; Schierz, A.; Trommler, U.; Horwitz, C.P.; Collins, T.J.; Kopinke, F.D. Humic acid modified Fenton reagent for enhancement of the working pH range. *Appl. Catal. B Environ.* **2007**, *72*, 26–36. [CrossRef]
35. Zeng, G.; Yang, R.; Habib, M.; Zhou, Z.; Xu, Z.; Sui, Q.; Lyu, S. Enhanced degradation of naphthalene in persulfate-based systems coupled with calcium sulfite: Elucidation of degradation mechanisms and pathways. *Sep. Purif. Technol.* **2024**, *330*, 125358. [CrossRef]
36. Gu, M.; Sui, Q.; Farooq, U.; Zhang, X.; Qiu, Z.; Lu, S. Degradation of phenanthrene in sulfate radical based oxidative environment by nZVI-PDA functionalized rGO catalyst. *Chem. Eng. J.* **2018**, *354*, 541–552. [CrossRef]